

Laser acceleration of monoenergetic protons via a double layer emerging from an ultra-thin foil

This article has been downloaded from IOPscience. Please scroll down to see the full text article.

2009 New J. Phys. 11 073006

(<http://iopscience.iop.org/1367-2630/11/7/073006>)

View [the table of contents for this issue](#), or go to the [journal homepage](#) for more

Download details:

IP Address: 130.159.82.166

The article was downloaded on 08/08/2013 at 12:00

Please note that [terms and conditions apply](#).

Laser acceleration of monoenergetic protons via a double layer emerging from an ultra-thin foil

Bengt Eliasson^{1,2,5}, Chuan S Liu³, Xi Shao³, Roald Z Sagdeev³
and Padma K Shukla^{2,4}

¹ Department of Physics, Umeå University, SE-90187 Umeå, Sweden

² Institut für Theoretische Physik IV, Fakultät für Physik und Astronomie,
Ruhr-Universität Bochum, D-44780 Bochum, Germany

³ Department of Physics, University of Maryland, College Park,
MD 20742, USA

⁴ Scottish Universities Physics Alliance, Department of Physics,
University of Strathclyde, Glasgow G4 ONG, UK

E-mail: bengt@tp4.rub.de

New Journal of Physics **11** (2009) 073006 (19pp)

Received 11 March 2009

Published 3 July 2009

Online at <http://www.njp.org/>

doi:10.1088/1367-2630/11/7/073006

Abstract. We present theoretical and numerical studies of the acceleration of monoenergetic protons in a double layer formed by the laser irradiation of an ultra-thin film. The ponderomotive force of the laser light pushes the electrons forward, and the induced space charge electric field pulls the ions and makes the thin foil accelerate as a whole. The ions trapped by the combined electric field and inertial force in the accelerated frame, together with the electrons trapped in the well of the ponderomotive and ion electric field, form a stable double layer. The trapped ions are accelerated to monoenergetic energies up to 100 MeV and beyond, making them suitable for cancer treatment. We present an analytic theory for the laser-accelerated ion energy and for the amount of trapped ions as functions of the laser intensity, foil thickness and the plasma number density. We also discuss the underlying physics of the trapped and untrapped ions in a double layer. The analytical results are compared with those obtained from direct Vlasov simulations of the fully nonlinear electron and ion dynamics that is controlled by the laser light.

⁵ Author to whom any correspondence should be addressed.

Contents

1. Introduction	2
2. Physics of thin foil acceleration	3
3. Comparison between theory and numerical modeling of the acceleration of a thin plasma slab	6
4. Summary and discussion	14
Acknowledgments	14
Appendix A. Simulation model	15
References	17

1. Introduction

The development of high power lasers has made it possible to study laser plasma interaction in the ultra relativistic regime, evidenced by the extensive literature on this subject [1, 2]. This has important effects on initial confinement fusion [3, 4] and high energy density physics. Particularly, the possibility of laser plasma acceleration of electrons, first proposed by Tajima and Dawson [5], has been experimentally verified [6] with hundreds of GeV cm^{-1} accelerating gradient. Even more significant for applications is the production of high quality, monoenergetic electron beam in the bubble regime of the plasma wake field, with short pulsed, high intensity lasers [7]–[16].

We therefore turn our interest to the possibility of laser acceleration of monoenergetic protons. The acceleration of ions by high power laser beams has attracted a great deal of attention due to its potential applications in fast ignition in inertial fusion research, proton radiography, medical isotope preparation, isochoric heating and cancer therapy [17]–[20]. For cancer treatment, deep-seated tumors require protons in excess of 200 MeV, which motivates the development of compact laser driven proton acceleration. Some experiments have reported quasi-monoenergetic ions [21]–[23] employing intricate and complex target designs.

A common method for accelerating ions is the target normal sheath acceleration (TNSA) [24, 25]. The nonlinear interactions of an ultrashort and ultra-intense (intensity of the order of $10^{21} \text{ W cm}^{-2}$) petawatt laser pulse and a thin foil target quickly ionizes the target, pushing a bunch of electrons from the ionized plasma foil due to the radiation pressure. As a result, a strong electrostatic field (of the order of terra-volts per meter) is set up between the expanding electron cloud and the rear of the plasma foil surface. Subsequently, the rear surface is ionized and protons are accelerated in the electrostatic field [26]–[32]. Generally one obtains broad spectrum of proton energy of the order of the ponderomotive pressure, typically multi MeV up to a few tens of MeV [33, 34]. Dong *et al* [35] investigated numerically the optimal thickness for ion emission using oblique incidence of the laser light and found that optimal thickness is when the foil becomes transparent to the laser light. Passoni and Lontano [36] have summarized recent experiments and have developed theoretical models to describe the profile of the accelerating field and to predict the energy spectra and maximum energy of the accelerated ions in the TNSA model. Esirkepov *et al* [37] presented a three-dimensional (3D) particle-in-cell (PIC) simulation study in the laser–piston regime, where the laser radiation pressure of linearly polarized waves is dominant. They demonstrated efficient relativistic ion generation, leading to ion beams with energies of hundreds of MeV or above. d’Humières *et al* [38] studied

plasma expansion and shock acceleration mechanisms by means of PIC simulations, while Yin *et al* [39] found a laser ‘break-out afterburner’ regime, where the laser penetrates the target and accelerates electron beams, which in turn accelerates the ions to hundreds of MeV by a relativistic Buneman instability.

Macchi *et al* [40] presented 1D and 2D PIC simulation studies where they observed high intensity ion bunches to be generated at the circularly polarized laser–plasma interaction surface and to be moving into the plasma. To obtain nearly monoenergetic ions, Klimo *et al* [41] Robinson *et al* [42] and Ryokovanov *et al* [43] considered the radiation pressure acceleration (RPA) of the thin film as a whole, using circular and linear polarization of the laser light. They demonstrated that circular polarization is crucial for efficient laser acceleration of a thin foil; in the case of linear polarization there is an oscillating component in the ponderomotive force term that leads to strong chaotic heating of the electrons followed by a foil explosion and broadening of the energy spectrum of the ions by the TNSA process. There is an optimal thickness of the target equal to the distance of maximum charge separation, suggested also by Yan *et al* [44]. Liseykina *et al* [45] presented a parametric numerical study of optimal target thickness for proton acceleration. The effects of multiple spatial dimensions on the stability of the accelerated foil have been investigated by Klimo *et al* [41], Robinson *et al* [42] and Pegoraro and Bulanov [46], showing that the foil can be fractured due to a Rayleigh–Taylor-like instability, leading to the bunching of the foil and the broadening of the ion energy spectrum. Properly tailored laser pulses with a sharp intensity rise may stabilize the foil and make it possible to efficiently accelerate monoenergetic proton beams in multiple dimensions [41, 46].

Yet some questions remain: how does the plasma maintain itself in such a seemingly stable state with density higher than a solid even in 1D? What traps the protons, preventing them from overshooting the electron front? Recently, we proposed [47] the self-organized double layer as a stably trapping mechanism in 1D. The electrons are trapped by the potential well formed by the balance of the radiation pressure and the electric force of the protons left behind, while protons are trapped in the accelerating frame by its inertial force while being accelerated by the electric field of the electron layer. This double layer allows the trapped protons to be accelerated as a monoenergetic group as the foil is accelerated by the radiation force as a whole. But a key question remains: what fraction of the protons are trapped and thus accelerated as monoenergetic ones? In this paper, we address these questions as well as the nature of proton trapping and test the role of the target thickness by employing an analytic and numerical study of the 1D Vlasov–Maxwell equations for protons and electrons.

2. Physics of thin foil acceleration

The acceleration of protons in a thin foil by intense laser light is based on the following physics. The foil is irradiated by an intense laser light that completely ionizes the foil to form a slab of plasma, and pushes the electrons forward towards the front end of the plasma slab by the radiation pressure. Einstein [48] first derived the radiation pressure for arbitrary incidence on a moving mirror using Lorentz transformation and the invariance of Maxwell’s equations. This work has been extended to arbitrary moving objects by Censor [49], and the subject also has been treated in textbooks [50, 51]. Debye [52] considered radiation pressure in his work on the physics of comets, while Marx [53] proposed that interstellar vehicles could be propelled by terrestrial laser beams. For our purposes, we will consider the radiation pressure of normal

incidence on a perfectly reflecting moving mirror [47]

$$F_{\text{rad}} = \frac{2I_0}{c} \left(\frac{1 - v/c}{1 + v/c} \right), \quad (1)$$

which takes into account the decrease of the radiation pressure due to the Doppler shift of the reflected light. Here I_0 is the intensity of the laser beam, v is the speed of the foil and c is the speed of light in vacuum. The ions are accelerated by the space-charge electric field induced by the separation of the electrons and ions in plasmas. This leads to an acceleration of the plasma slab as a whole by the radiation pressure. The RPA has been discussed earlier in [37, 42, 53]. We assume a thin plasma slab of an equal number N_0 of the ions and electrons, so that its total rest mass density is $N_0 m_i$, where m_i is the ion rest mass, in a 1D geometry along the z -axis. The equation of motion for the plasma slab is then

$$\frac{d(\gamma v)}{dt} = \frac{F_{\text{rad}}}{N_0 m_i} = \frac{cP}{T_L} \left(\frac{1 - v/c}{1 + v/c} \right), \quad (2)$$

where T_L is the temporal laser period, $\gamma = (1 - v^2/c^2)^{-1/2}$ is the relativistic gamma factor, and we have denoted the dimensionless parameter

$$P = \frac{2T_L I_0}{N_0 m_i c^2}. \quad (3)$$

Equation (2) can be integrated to give the speed [47]

$$\frac{v(t)}{c} = \frac{g(t)^2 - 1}{g(t)^2 + 1}, \quad (4)$$

where $g = \{2^{1/3}[h(t) + \sqrt{4 + h(t)^2}]^{2/3} - 2\} / \{2^{2/3}[h(t) + \sqrt{4 + h(t)^2}]^{1/3}\}$ and $h(t) = 6Pt/T_L + 4$. The position $z(t)$ of the plasma slab (center of mass position) is found from $dz/dt = v$, which combined with (2) yields

$$\frac{d(\gamma v)}{dz} = \frac{cP}{T_L v} \left(\frac{1 - v/c}{1 + v/c} \right). \quad (5)$$

Integration of equation (5) gives

$$\frac{z(t)}{\lambda_L} = \frac{1}{6P} \left[\left(\frac{1 + v/c}{1 - v/c} \right)^{3/2} - 3 \left(\frac{1 + v/c}{1 - v/c} \right)^{1/2} + 2 \right], \quad (6)$$

where v is given by (4).

The kinetic energy of a typical ion in the slab is

$$\mathcal{E}_i = m_i c^2 (\gamma - 1). \quad (7)$$

These are the ions trapped in a self-organized double layer that is formed by the balance of the electrostatic attractive potential of the electrons and the inertial force of the accelerating frame. These trapped ions form a blob of monoenergetic ions in phase space.

Now we wish to examine the conditions for the validity of the assumption of plasma slab accelerated as a whole, pushed by the radiation pressure, since the slab is in fact a plasma. The rigidity is due to the formation of a self-arranged accelerated double layer, which traps the ions and electrons. The formation of the electron layer is due to the balance between the laser ponderomotive force pushing the electrons forward and the electrostatic force by the ions behind, pulling the electrons back. For the ion layer, it is the balance between the electrostatic

force of the electrons accelerating them and the inertial force of the acceleration holding them back. The effective potential well of the double layer traps the ions and moves them together as a whole system, which is accelerated by the radiation pressure.

Due to the acceleration, there will also be a group of ions that are untrapped and left behind the accelerated layer, making the plasma slab negatively charged. An ion will be untrapped if the acceleration by the space charge electric field is weaker than the mean acceleration of the whole plasma slab. It is interesting to consider the forces on an ion in the moving frame of the foil accelerated by the laser radiation. In this frame, there will be an accelerating force by the electrostatic field and a decelerating inertial force. The balance between these two forces determines whether the ions will be trapped or untrapped. Hence, we can define the effective potential as a sum of the electrostatic and inertial potentials, $\phi'(z, t) = \phi(z, t) + (F_{\text{rad}}/eN_0)z$. In a frame moving with the speed $v(t)$ of the foil, the equation of motion for the ion is then given by

$$m_i \frac{d(\gamma_i v_i)}{dt} = -e \frac{\partial \phi'}{\partial z} = eE - \frac{F_{\text{rad}}}{eN_0}, \quad (8)$$

where $E = -\partial\phi/\partial z$ is the electric field.

For applications of the ion acceleration, it is interesting to estimate how large a portion of the ions is trapped in the plasma slab and are accelerated to monoenergetic energies and how many ions are untrapped and spread out in energy. The loss of the ions will stop when the electric field behind the plasma slab is large enough, say due to untrapped ions, so that the acceleration of an ion by this electric field is as large as the mean acceleration of the plasma slab. We assume a thin plasma slab of initially an equal number of ions and electrons, in a 1D geometry along the z -axis. Then the electric field behind the accelerated layer is obtained from the Poisson equation $\partial E/\partial z = en_i/\epsilon_0$ as

$$E_{\text{un}} = \frac{eN_{\text{un}}}{\epsilon_0}, \quad (9)$$

where $N_{\text{un}} = \int_0^{z_0} n_i dz$ is the integrated (along the z -axis) number of untrapped ions and z_0 is the boundary between trapped and untrapped ions. Using $E = E_{\text{un}}$ in (8), we have

$$m_i \frac{d(\gamma_i v_i)}{dt} = \frac{eN_{\text{un}}}{\epsilon_0} - \frac{F_{\text{rad}}}{eN_0}. \quad (10)$$

If the right-hand side of (10) is larger than zero, then the ion is falling into the potential well and can be considered as trapped, while if it is less than zero, it can be considered as untrapped. The number of trapped ions can be found when $m_i d(\gamma_i v_i)/dt = 0$, yielding

$$\frac{N_{\text{un}}}{N_0} = \frac{\epsilon_0}{e^2 N_0^2} F_{\text{rad}}. \quad (11)$$

The fraction of the number of trapped ions to the total number of ions is

$$\frac{N_{\text{tr}}}{N_0} = 1 - \frac{\epsilon_0}{e^2 N_0^2} F_{\text{rad}}. \quad (12)$$

In particular, we note that all ions are untrapped ($N_{\text{un}} = N_0$) when

$$F_{\text{rad}} = \frac{e^2 N_0^2}{\epsilon_0}, \quad (13)$$

and for $F_{\text{rad}} > e^2 N_0^2 / \epsilon_0$, one would have a complete separation between the electrons and ions. In this case, the electrons will be accelerated in front of the ions by the radiation pressure, while the left-behind ions will experience a Coulomb explosion due to the electrostatic repulsion. This will result in a large spread in ion energies and will decrease the usefulness of these ions in applications where monoenergetic ions are needed.

3. Comparison between theory and numerical modeling of the acceleration of a thin plasma slab

To assess the validity of the present theory, we have performed a series of Vlasov simulations and have compared the numerical results with those deduced from analytical formulae presented in section 2. While many simulation studies of proton acceleration have been carried out using PIC simulations, we believe that this is the first time a grid-based Vlasov solver has been used for this purpose. Therefore, it is worthwhile to discuss the difference between the two methods. In the PIC method [54], the Vlasov equation is solved by following the trajectories of a set of statistically distributed super-particles, which resolves the particle distribution functions in phase space. Each super-particle represents a large number of real particles. PIC simulations have proven to be extremely successful due to their relative simplicity and adaptivity, especially in problems involving large-amplitude waves and beams, and in multiple spatial dimensions. However, the statistical noise of PIC simulations sometimes overshadows the physical results, and for some problems, the low-density velocity tail of the particle distribution cannot be resolved with high enough accuracy by the super-particles. As a contrast, the grid-based Vlasov solver treats the particle distribution function as a continuous phase fluid that is represented on a grid in both space and velocity (or momentum) space. The advantage with grid-based Vlasov solvers is that there is no statistical noise in the simulations, and that the dynamical range is determined by the number system of the computer rather than super particles. Hence, the low-density velocity tail of the particle distribution can be resolved much more accurately by grid-based Vlasov solvers, which makes them suitable for certain types of problems. Simulations in higher dimensions using grid-based Vlasov solvers are very challenging since the full phase-space has to be represented on a grid, which makes both the storage of the data in the computer's memory, and the numerical calculations, extremely demanding. One also has to be aware of the tendency of the distribution function to become oscillatory in velocity space, which can lead to unphysical noise and recurrence effects in the numerical solution unless proper smoothing or viscosity is used in velocity space [55]. In our simulations, we used proper numerical viscosity in configuration space and momentum space to minimize these effects.

Let us present the relevant nonlinear kinetic model describing the proton acceleration resulting from the nonlinear interaction between intense laser light and a collisionless plasma. A more detailed derivation of the governing equations is given in the appendix. The electromagnetic wave gives rise to the relativistic electron mass increase $m_e \gamma_e$ and a relativistic ponderomotive force [1], $F_e = -m_e c^2 \partial \gamma_e / \partial z$, where m_e is the electron rest mass, and $\gamma_e = (1 + p_z^2 / m_e^2 c^2 + e^2 |\mathbf{A}|^2 / m_e^2 c^2)^{1/2}$ is the relativistic electron gamma factor and p_z is the z component of the electron momentum. The relativistic ion mass is $m_i \gamma_i$, and the ponderomotive force acting on the ions reads $F_i = -m_i c^2 \partial \gamma_i / \partial z$, where m_i is the ion rest mass and $\gamma_i = (1 + p_z^2 / m_i^2 c^2 + e^2 |\mathbf{A}|^2 / m_i^2 c^2)^{1/2}$ is the relativistic ion gamma factor. For the ions, the relativistic effects due to the quivering of the ions in the radiation field (proportional to $|\mathbf{A}|^2$ inside the ion gamma factor) can usually be neglected due to the large mass of the ions compared to that of the electrons.

The complex envelope of the perpendicular (to the z -axis) vector potential of the circularly or linearly polarized electromagnetic wave is given by the wave equation

$$\left(\frac{\partial}{\partial t} - i\omega_0\right)^2 A - c^2 \frac{\partial^2 A}{\partial z^2} + \Omega_p^2 A = 0, \quad (14)$$

where

$$\Omega_p^2 = \frac{e^2}{\epsilon_0} \int \left(\frac{f_e}{m_e \gamma_e} + \frac{f_i}{m_i \gamma_i} \right) dp_z \quad (15)$$

is the local plasma frequency, accounting for the relativistic mass increase and plasma density variations, and ω_0 is the laser angular frequency. For circularly polarized light, we will have $|\mathbf{A}|^2 = |A|^2$, where we note that the oscillatory part of the light cancel exactly. On the other hand, for linear polarization, we would instead have $|\mathbf{A}|^2 = |A|^2 [1 + \cos(2\omega_0 t - 2\phi)]/2$, where ϕ is the complex phase of A . We note that in this case, $|\mathbf{A}|^2$ has an oscillatory part with a frequency twice that of the laser light, which will enter into the ponderomotive force for the electrons [42, 43]. We will consider circularly polarized light below unless stated otherwise.

The parallel electric field is obtained from the Maxwell equation

$$\frac{\partial E_z}{\partial t} = \frac{e}{\epsilon_0} \int p_z \left(\frac{f_e}{m_e \gamma_e} - \frac{f_i}{m_i \gamma_i} \right) dp_z, \quad (16)$$

with initial conditions obtained from Gauss' law

$$\frac{\partial E_z}{\partial z} = -\frac{\partial^2 \phi}{\partial z^2} = \frac{\rho}{\epsilon_0}, \quad (17)$$

where we have introduced the electrostatic potential ϕ and

$$\rho = e \int (f_i - f_e) dp_z \quad (18)$$

is the electric charge density. The electromagnetic field is coupled nonlinearly with the ions and electrons, whose dynamics is governed by the ion and electron Vlasov equations in the lab frame

$$\frac{\partial f_i}{\partial t} + \frac{p_z}{m_i \gamma_i} \frac{\partial f_i}{\partial z} + \frac{\partial(-e\phi - m_i c^2 \gamma_i)}{\partial z} \frac{\partial f_i}{\partial p_z} = 0 \quad (19)$$

and

$$\frac{\partial f_e}{\partial t} + \frac{p_z}{m_e \gamma_e} \frac{\partial f_e}{\partial z} + \frac{\partial(e\phi - m_e c^2 \gamma_e)}{\partial z} \frac{\partial f_e}{\partial p_z} = 0, \quad (20)$$

respectively. Equations (14), (16), (19) and (20) form a closed set for our purposes. Similar models have been used to study electron phase-space structures [56]–[59].

In our simulations, we used a simulation box in z space of size $200c/\omega_0$, which was resolved with 2000 grid points. For the electrons, we used a momentum space spanning $\pm 10m_e c$, resolved with 60 grid points, while the ion momentum space was taken from $-30m_e c$ to $+1470m_e c$, resolved with 6000 grid points. We used absorbing boundary conditions for the Vlasov equations such that the electrons or ions hitting the right or left boundary were absorbed and removed from the simulation. For the electromagnetic wave, we used an outflow boundary condition on the right boundary, the electromagnetic wave of amplitude A_0 was

injected at the left boundary while absorbing outgoing waves. The initial conditions for the ions and electrons were taken to be a Maxwellian distribution of the form $f_{i,e}(z, p_z)_{t=0} = \{n_{i,e}(z)/[(2\pi)^{1/2}\alpha_{i,e}]\}\exp[-p_z^2/2\alpha_{i,e}^2]$ with $\alpha_i = 0.8 m_e c$ and $\alpha_e = 0.4 m_e c$, and with the initial ion and electron number density $n_{i,e} = n_0$ in the interval $-L/2 < z < L/2$ and $n_{i,e} = 0$ elsewhere. In our computer simulations, we used a compact Padé scheme [60] to approximate the p_z and x derivatives, while we used the standard fourth-order Runge–Kutta scheme for the time-stepping.

The laser intensity is related to the laser amplitude through

$$I_0 = \epsilon_0 \omega_0^2 A_0^2 c = \frac{\epsilon_0 \omega_0^2 m_e^2 c^3}{e^2} a_0^2, \quad (21)$$

where $a_0 = e|A_0|/m_e c$ is the normalized amplitude of the injected laser light. We assume a thin plasma slab with the electron number density n_0 and the width L , so that the total number of ions is $N_0 = n_0 L$. In terms of these parameters, the dimensionless parameter P in (3) is

$$P = \frac{2T_L I_0}{n_0 L m_i c^2} = 2 \frac{m_e}{m_i} \frac{\omega_0^2}{\omega_{pe}^2} \frac{\lambda_L}{L} a_0^2, \quad (22)$$

where $\omega_{pe} = (n_0 e^2 / \epsilon_0 m_e)^{1/2}$ is the plasma frequency of the overdense plasma slab, $\lambda_L = 2\pi c / \omega_0$ is the laser wavelength in vacuum, ω_0 is the laser angular frequency and $m_i / m_e = 1836$ is the proton to electron mass ratio. In terms of our parameters, the expression for the fraction of the trapped ions (12) can be written as

$$\frac{N_{tr}}{N_0} = 1 - \frac{2}{(2\pi)^2} \frac{\omega_0^4}{\omega_{pe}^4} \frac{\lambda_L^2}{L^2} \left(\frac{1-v/c}{1+v/c} \right) a_0^2. \quad (23)$$

We note that the fraction of the trapped ions is smallest initially when the speed of the foil v is small and increases for larger values of v . Hence, a fraction of the ions initially untrapped may later catch up and again become trapped. In our simulations, we used a plasma slab whose density n_0 was 10 times larger than the critical density $n_c = \epsilon_0 m_e^2 \omega_0^2 / e^2$ of the laser light, so that $\omega_{pe}^2 / \omega_0^2 = 10$, and a laser amplitude of $a_0 = 5$. We made three runs with different initial thicknesses of the plasma slab, with thickness $L = 0.1\lambda_L$, $L = 0.2\lambda_L$ and $L = 0.4\lambda_L$. We note from (23) that if

$$a_0^2 > \frac{(2\pi)^2}{2} \frac{\omega_{pe}^4}{\omega_0^4} \frac{L^2}{\lambda_L^2}, \quad (24)$$

no ions will be initially trapped and the theory predicts a separation between the electron and ion layers. For $\omega_{pe}^2 / \omega_0^2 = 10$, the electron and ion layers will be separated if $a_0 > 4.5$ for $L = 0.1\lambda_L$, $a_0 > 9$ for $L = 0.2\lambda_L$, and $a_0 > 18$ for $L = 0.4\lambda_L$. Hence, for the chosen value $a_0 = 5$, we are above the threshold for complete separation of the electron and ion layers for the thinnest slab $L = 0.1\lambda_L$, while we are below the threshold for $L = 0.2\lambda_L$ and $L = 0.4\lambda_L$.

We first discuss the case $L = 0.2\lambda_L$. This is close to the optimal thickness $L = (\omega_0^2 / \omega_{pe}^2) a_0 \lambda_L / \pi \approx 0.16\lambda_L$ for the monoenergetic ion acceleration [47]. In figures 1–4, we have presented details of the simulations at different times. At time $t = 3.4 T_L$, we see in figure 1(a) that the laser amplitude has set up a standing wave pattern behind the plasma layer, with an amplitude of $a \approx 10$ of its first maximum, i.e. 2 times that of the injected wave. A small portion of the laser light, with an amplitude of $a \approx 1$, has also tunneled through to the right side of the plasma layer. The electrons, seen in figure 1(b), are pushed forward by the laser light but

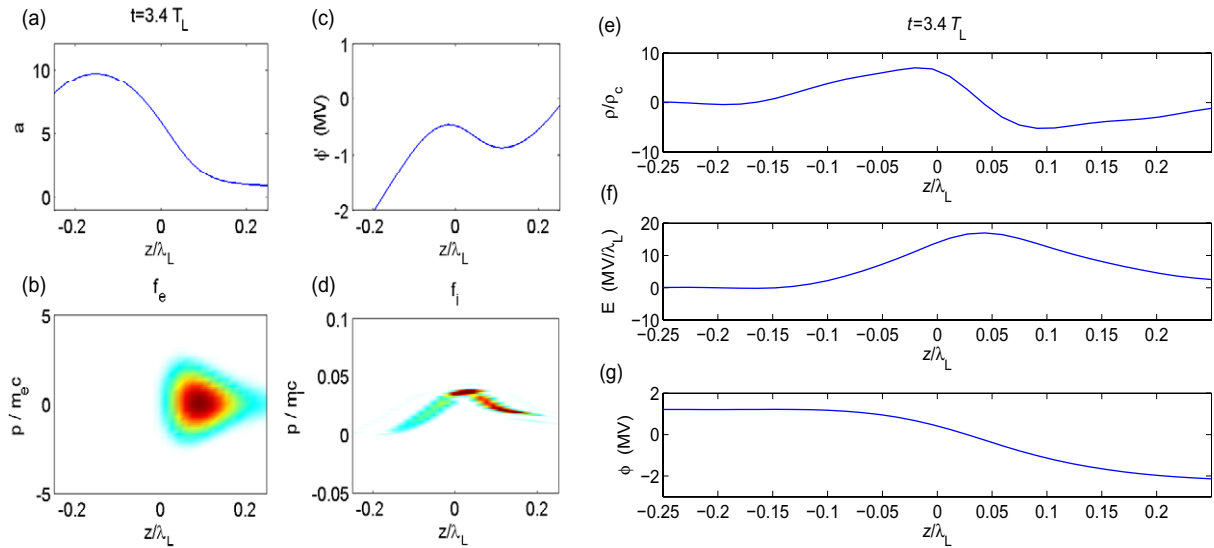


Figure 1. Simulation results at $t = 3.4 T_L$, for slab thickness $L = 0.2 \lambda_L$: (a) the laser amplitude, (b) the electron distribution function, (c) the effective potential, (d) the ion distribution function, (e) the charge density normalized by $\rho_c = en_c$, (f) the electric field and (g) the electric potential.

are kept back by the space charge electric field. The charge density in figure 1(e) shows a bipolar structure where the left-hand side is positively charged and the right-hand side negatively charged, giving rise to the localized positive electric field in figure 1(f) and the associated double-layer structure of the potential in figure 1(g). The effective trapping potential for the ions given in equation (8), which is derived from the sum of the electrostatic and inertial forces, is depicted in figure 1(c). The latter shows a local minimum at $z \approx 0.1 \lambda_L$ and a maximum at $z \approx 0$. The ions that are to the left of the potential maximum are starting to lag behind the accelerated plasma layer, and can be considered as untrapped. In figure 1(c), we see a bunch of monoenergetic ions at $z = 0$, which coincide with the left edge of the electron layer in figure 1(b). This ion bunch is accelerated uniformly by the space charge electric field.

At $t = 16 T_L$, displayed in figure 2, the effective potential has deepened and broadened further with a minimum at $z = 1.5 \lambda_L$ and the local maximum at $z = 1 \lambda_L$, making the trapped ions more deeply trapped. The untrapped population of the ions, clearly seen in figure 2(d) between $z = 0$ and $z = 1.5 \lambda_L$, form an almost homogeneous positive charge density seen in figure 2(e) and associated linearly increasing positive electric field and concave potential profile, seen in figures 2(f) and (g). Note that most of the ions are trapped in the bottom of the effective potential well at $z = 1.5 \lambda_L$. They have reached a momentum of $\sim 0.2 m_i c$, corresponding to an energy of ~ 20 MeV.

Turning to the results at $t = 35 T_L$, shown in figure 3, we observe that the effective potential has deepened and broadened further. Here, the trapped protons have been accelerated to momenta of $0.35 m_i c$ corresponding to a proton energy of ~ 55 MeV. We see in figure 3 that a portion of the previously untrapped ions begin to fall into the potential and to overtake the trapped ion population at $z \approx 6.5 \lambda_L$. This is due to the decrease of the radiation pressure at higher speeds of the plasma layer by the Doppler shift of the reflected light, giving rise to the factor $(1 - v/c)/(1 + v/c)$ in the expression for the radiation pressure (1) and in the equation of motion (2). Also here the untrapped population of the ions, seen in figure 3(d) gives rise to

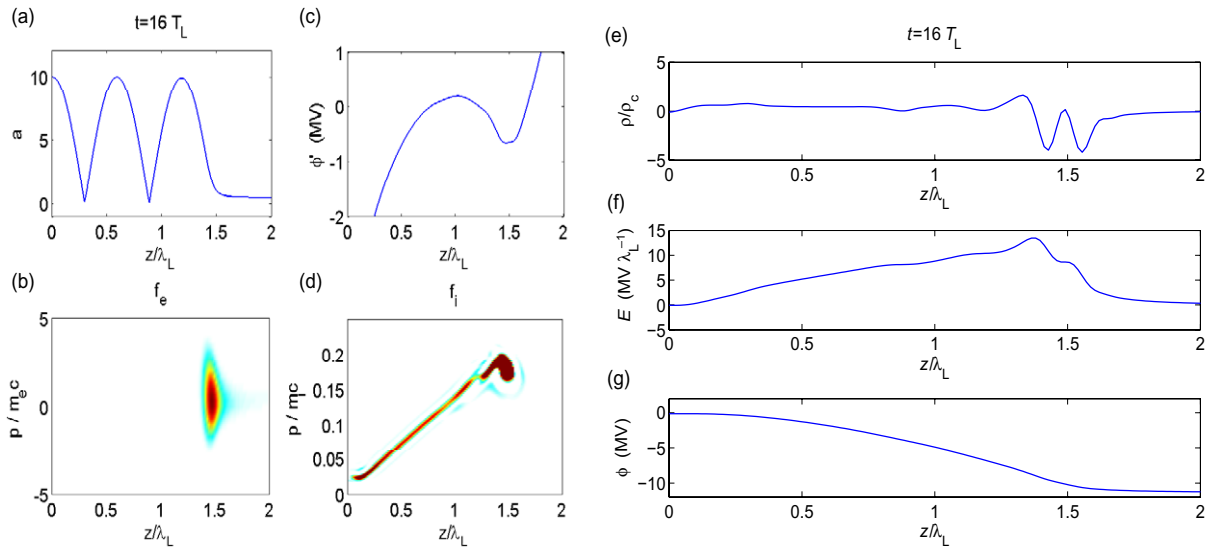


Figure 2. Simulation results at $t = 16 T_L$, for slab thickness $L = 0.2 \lambda_L$: (a) the laser amplitude, (b) the electron distribution function, (c) the effective potential, (d) the ion distribution function, (e) the charge density, (f) the electric field and (g) the electric potential.

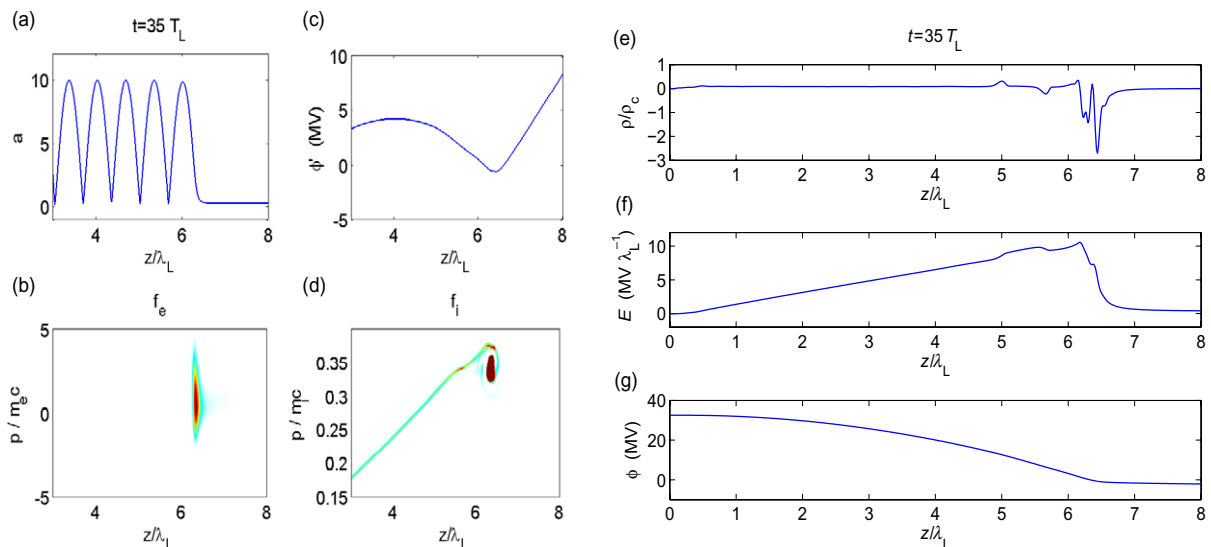


Figure 3. Simulation results at $t = 35 T_L$, for slab thickness $L = 0.2 \lambda_L$: (a) the laser amplitude, (b) the electron distribution function, (c) the effective potential, (d) the ion distribution function, (e) the charge density, (f) the electric field and (g) the electric potential.

a linearly increasing positive electric field and concave potential profile, as seen in figures 3(f) and (g).

At $t = 73 T_L$, shown in figure 4, the trapped protons have been accelerated to momenta of $0.55 m_i c$ corresponding to a proton energy of ~ 130 MeV. We see in figure 4(d) that previously trapped ions continue to fall into the effective potential minimum and become re-trapped.

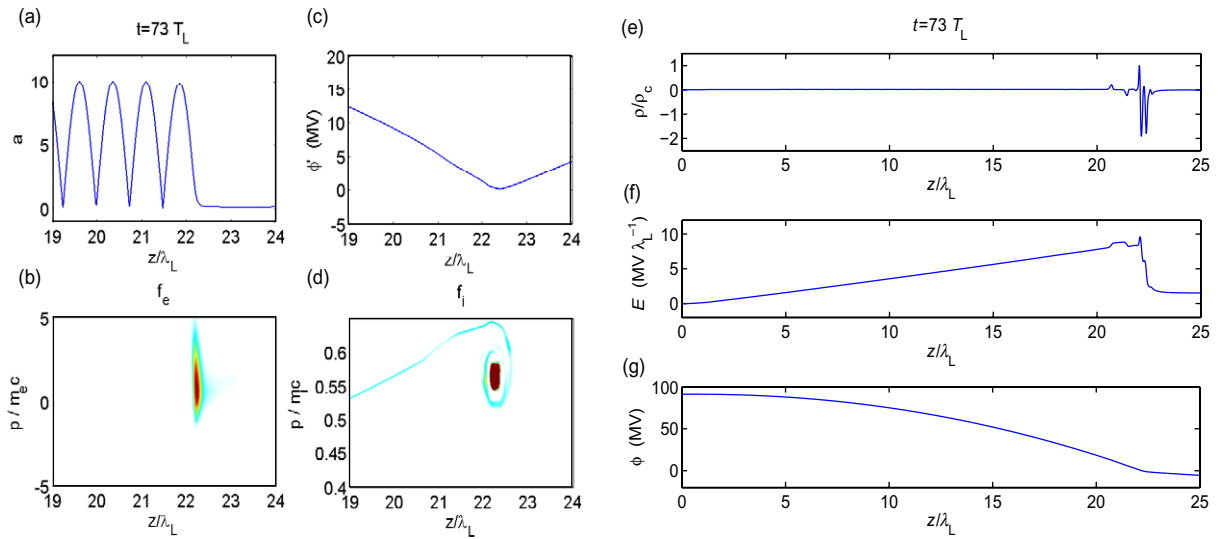


Figure 4. Simulation results at $t = 73 T_L$, for slab thickness $L = 0.2 \lambda_L$: (a) the laser amplitude, (b) the electron distribution function, (c) the effective potential, (d) the ion distribution function, (e) the charge density, (f) the electric field and (g) the electric potential.

For the thinnest plasma slab, $L = 0.1 \lambda_L$, illustrated in figure 5, we observe that a few laser periods after the laser light has reached the plasma slab, the electrons have not been separated from the ions, but instead the laser light is tunneling through the plasma barrier. The normalized amplitude $a = e|A|/m_e c$ of the laser light is of the order $a \approx 5$ inside the electron slab, so that the relativistic electron mass increase is a factor ≈ 5 , making the plasma less overdense and the thin layer almost completely optically transparent. At this point, the proton acceleration stops and the fastest protons have gained energy of only ~ 0.2 MeV.

Finally, we display the results with the thicker slab $L = 0.4 \lambda_L$ at $t = 73 T_L$ in figure 6. We see that the accelerated ions are less coherent with a larger spread in momentum (and ion energy) than for the thinner foil in figure 4. Initially, we, similarly to Macchi *et al* [40], observed ‘pulsed’ acceleration and the production of ion bunches directed towards the plasma slab. The acceleration is slower due to the larger inertial of the thicker slab in figure 6. Here, we could measure that about 95% of the ions are trapped in the effective potential well.

In the RPA discussed here, the laser beam accelerates the whole plasma slab (ions + electrons) as a whole. For this to work, we clearly need the electron pressure to be sufficiently low so that the plasma slab does not expand by the electron thermal pressure to make the foil transparent, and thus circularly polarized light is preferred since this minimizes the electron heating. Hence, the radiation pressure should be larger than the electron thermal pressure, $2I_0/c > n_0 T_e$. From the electron distribution function (panel b in figures 1–4 and 6), we can estimate the electron thermal energy to be of the order $T_e \sim 1 m_e c^2$, which should be less than (using the expression (21) for I_0), $2I_0/(n_0 c) = 2\epsilon_0 \omega_0^2 m_e^2 c^3 a_0^2 / (e^2 n_0 c) = 2(\omega_0^2 / \omega_{pe}^2) a_0^2 m_e c^2 = 5 m_e c^2$, for our parameters $\omega_0^2 / \omega_{pe}^2 = 1/10$ and $a_0 = 5$. Hence, the radiation pressure is here ~ 5 times larger than the electron thermal pressure and the foil is prevented from undergoing thermal expansion. For the electrons, we instead have a balance between the radiation pressure and the electrostatic force as discussed above.

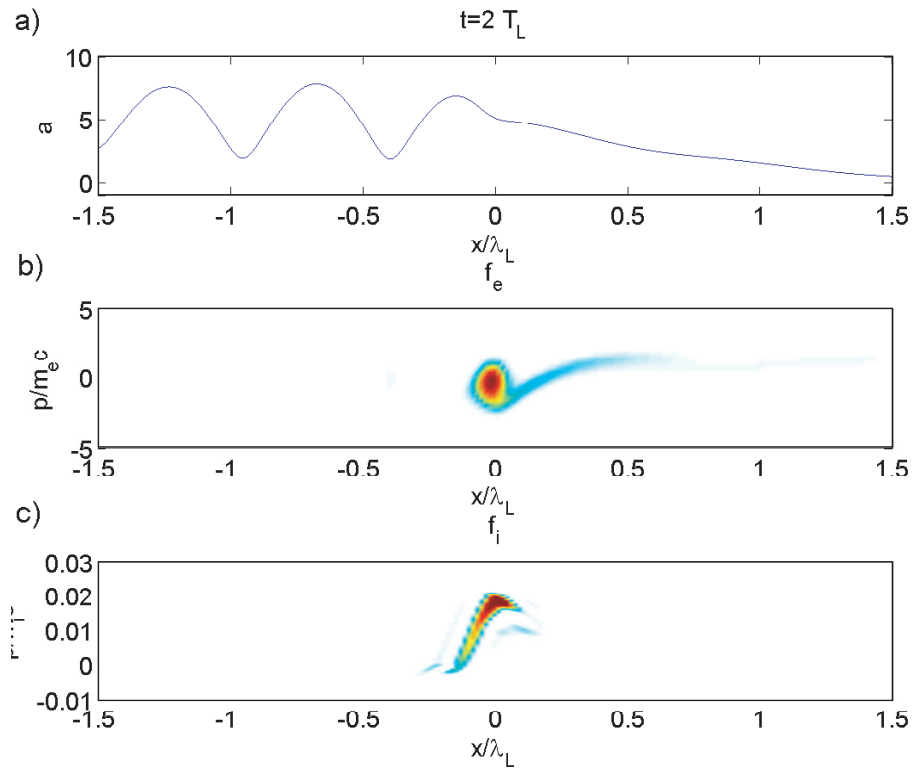


Figure 5. Simulation results at $t = 2 T_L$, for slab thickness $L = 0.1 \lambda_L$: (a) the laser amplitude, (b) the electron distribution function and (d) the ion distribution function.

It is interesting to compare the theoretical prediction of the energy (7) as a function of time and space (6) to the ones obtained via our Vlasov simulations. The latter is obtained by recording the mean position of the trapped ion bunch in phase-space (z_i , p_i), seen in panel (d) in figures 1–4, at each time t and use that energy of a trapped ion, which is given by $\mathcal{E}_i = m_i c^2 (\sqrt{1 + p_i^2 / m_i^2 c^2} - 1)$. The comparison, displayed in figure 7, shows excellent agreement between the theoretical prediction and the numerical results, both for $L = 0.2 \lambda_L$ and $L = 0.4 \lambda_L$.

In figure 8, we have integrated the trapped ions over momentum space and displayed the fraction of the trapped ions obtained in the Vlasov simulations for $L = 0.2 \lambda_L$ and $L = 0.4 \lambda_L$ as a function of time. We see in figure 8 that about 75–80% of the ions are trapped in the simulation for $L = 0.2 \lambda_L$, and about 95% are trapped for $L = 0.4 \lambda_L$. This is approximately what is predicted by equation (23) at small speeds ($v \ll c$). As the accelerated layer increases in speed, the efficiency of the radiation pressure decreases due to the Doppler shift effect. This means that a portion of the untrapped ions starts to overtake the accelerated layer and to be re-trapped as discussed in figures 4 and 6. However, the re-trapping of the untrapped ions is a relatively slow process and we see only a slight increase of the trapped ions in the simulations at later times, where the formula (23) tends to overestimate the number of the trapped ions at later times.

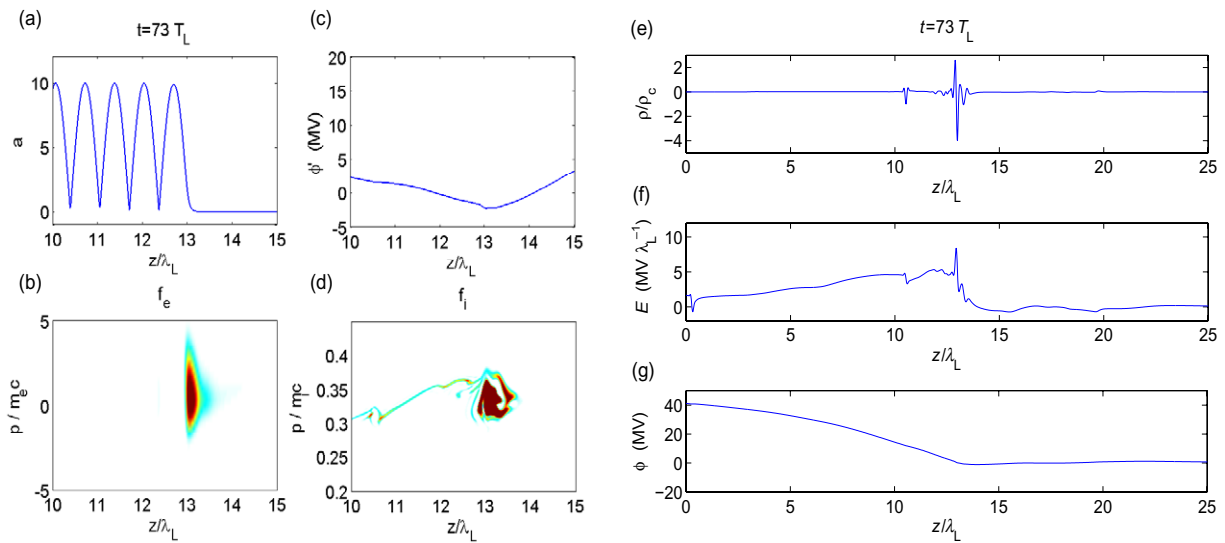


Figure 6. Simulation results at $t = 73 T_L$, for slab thickness $L = 0.4 \lambda_L$: (a) The laser amplitude, (b) the electron distribution function, (c) the effective potential, (d) the ion distribution function, (e) the charge density, (f) the electric field and (g) the electric potential.

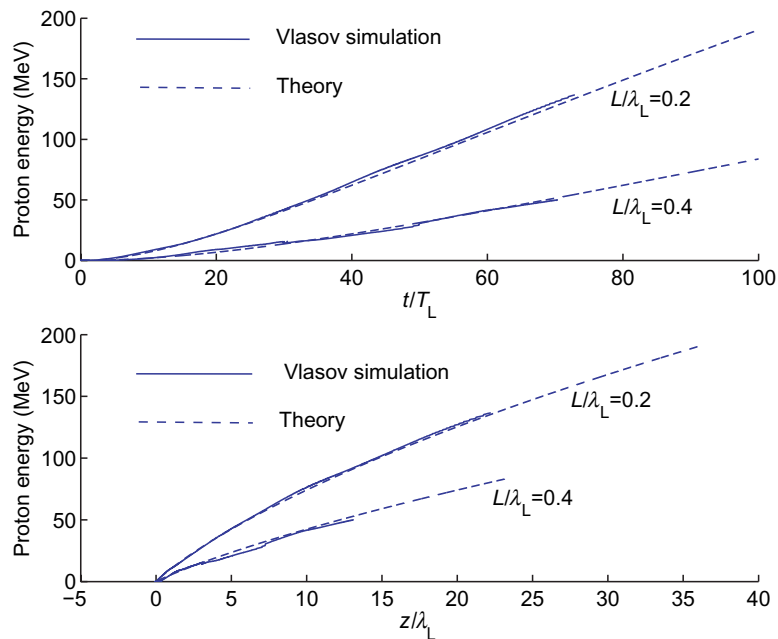


Figure 7. The proton energy versus time (top panel) and space (bottom panel), theoretical model (dashed lines) and Vlasov simulation (solid lines), for the slab thicknesses $L/\lambda_L = 0.2$ and $L/\lambda_L = 0.4$.

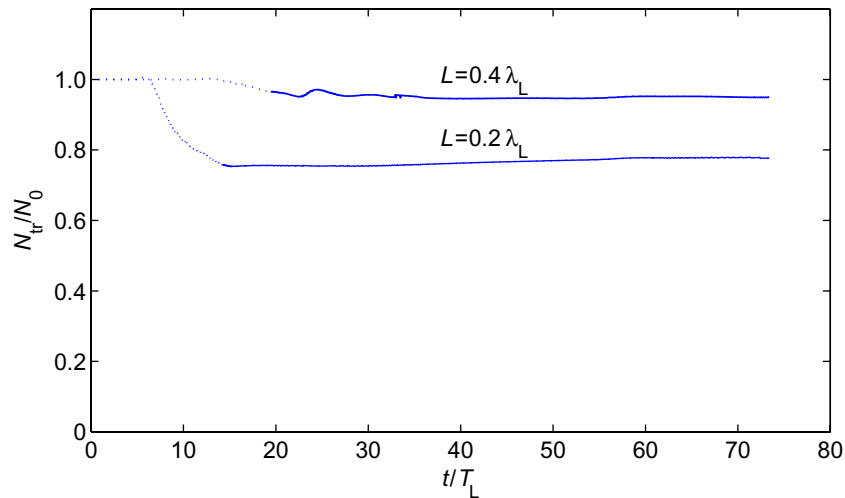


Figure 8. The fraction of trapped ions as a function of time in the Vlasov simulations for slab thickness $L/\lambda_L = 0.2$ and $L/\lambda_L = 0.4$. The dotted lines indicate the initial stage of the acceleration before the trapped and untrapped ions can be distinguished.

4. Summary and discussion

In summary, we have presented theoretical and numerical studies of ion acceleration in an ultra-thin plasma foil by intense laser light. In the RPA, the radiation pressure pushes the electrons forward into the foil until they are stopped by the induced space-charge electric field. On the other hand, the electric field accelerates the ions, which are held back by the inertial force in the accelerated frame. As a result, both the electrons and ions are trapped, and the thin foil is accelerated as a whole. We have derived analytic formulae for the ion energy of the trapped ions, which depend on the laser intensity and its duration, foil thickness and the plasma number density. Also discussed is the physics of trapped and untrapped ions in the double layer, where, due to the acceleration, some ions are untrapped and spread out in energy. The obtained theoretical results show excellent agreement when compared against direct Vlasov–Maxwell simulations of the ion and electron dynamics in the laser field. Our numerical Vlasov simulation results are generally in agreement with previous works using PIC simulations. The present investigation indicates that monoenergetic ions can be accelerated to energies of the order of 100 MeV in 100 laser periods, making them suitable for medical treatment. Even though investigations in multiple dimensions show that the foil is unstable to a Rayleigh–Taylor-like instability [41, 42, 46], properly tailored laser pulses may stabilize the foil long enough to accelerate it efficiently [46]. Klimo’s work [41] also show that the acceleration of ~ 100 MeV quasi-monoenergetic proton beams remains a possibility in multiple dimensions. Further investigations are underway and will be published elsewhere.

Acknowledgments

This work was partially supported by the Deutsche Forschungsgemeinschaft through the project SH 21/3-1 of the Research Unit 1054, and by the Swedish Research Council (VR).

BE acknowledges the support and hospitality of the University of Maryland where this work was carried out.

Appendix A. Simulation model

Here, we summarize the derivation of the relevant equations describing nonlinear interactions between intense laser light and a collisionless plasma. The electromagnetic field is governed by Faraday's and Ampère–Maxwell's equations

$$\frac{\partial \mathbf{B}}{\partial t} = -\nabla \times \mathbf{E} \quad (\text{A.1})$$

and

$$\frac{\partial \mathbf{E}}{\partial t} = c^2 \nabla \times \mathbf{B} - \frac{e}{\epsilon_0} \int (\mathbf{v}_i f_i - \mathbf{v}_e f_e) d^3 p, \quad (\text{A.2})$$

respectively, where f_i and f_e are the ion and electron distribution functions, and $\mathbf{v}_j = \mathbf{p}/m_j \gamma_j$ is the velocity of the particle species j (j equals i for the ions and e for the electrons), and $\gamma_j = [1 + (p_x^2 + p_y^2 + p_z^2)/m_j^2 c^2]^{1/2}$ is the relativistic gamma factor, together with the Gauss law

$$\nabla \cdot \mathbf{E} = \frac{e}{\epsilon_0} \int (f_i - f_e) d^3 p \quad (\text{A.3})$$

and the divergence condition on the magnetic field

$$\nabla \cdot \mathbf{B} = 0. \quad (\text{A.4})$$

We will consider a 1D geometry along the z -axis. In this geometry, it is convenient to introduce the scalar and vector potentials, ϕ and \mathbf{A} , respectively, through their relations to the electric and magnetic fields

$$\mathbf{E} = -\frac{\partial \phi}{\partial z} \hat{\mathbf{z}} - \frac{\partial \mathbf{A}}{\partial t} \quad (\text{A.5})$$

and

$$\mathbf{B} = \hat{\mathbf{z}} \times \frac{\partial \mathbf{A}}{\partial z}, \quad (\text{A.6})$$

where \mathbf{A} is the vector potential of the electromagnetic wave, which in the Coulomb gauge ($\nabla \cdot \mathbf{A} = 0$) is given by $\mathbf{A} = \hat{\mathbf{x}} A_x + \hat{\mathbf{y}} A_y$. Here $\hat{\mathbf{x}}$, $\hat{\mathbf{y}}$ and $\hat{\mathbf{z}}$ are the unit vectors along the x , y and z directions in a Cartesian coordinate system. We then have from the Gauss law

$$\frac{\partial E_z}{\partial z} = -\frac{\partial^2 \phi}{\partial z^2} = \frac{e}{\epsilon_0} (n_i - n_e) \quad (\text{A.7})$$

and the parallel (to $\hat{\mathbf{z}}$) and perpendicular components of the Ampère–Maxwell laws

$$\frac{\partial E_z}{\partial t} = \frac{e}{\epsilon_0} \int (v_{ez} f_e - v_{iz} f_i) d^3 p \quad (\text{A.8})$$

and

$$\frac{\partial^2 \mathbf{A}}{\partial t^2} - c^2 \nabla^2 \mathbf{A} = \frac{e}{\epsilon_0} \int \mathbf{v}_\perp (f_e - f_i) d^3 p, \quad (\text{A.9})$$

respectively.

In our kinetic model for the electrons and ions, we will use (A.5) and (A.6) together with the particle momentum equation to obtain

$$\frac{d\mathbf{p}_j}{dt} = q_j(\mathbf{E} + \mathbf{v}_j \times \mathbf{B}) = -q_j \frac{d\mathbf{A}}{dt} - q_j \frac{\partial \phi}{\partial z} \hat{\mathbf{z}} + \frac{q_j}{\gamma_j m_j} \mathbf{p}_j \cdot \frac{\partial \mathbf{A}}{\partial z} \hat{\mathbf{z}}, \quad (\text{A.10})$$

for the particle species j , where the electric charge $q_i = e$ and $q_e = -e$ and the total derivative $d/dt = \partial/\partial t + v_{zj} \partial/\partial z$. Hence, we can take the perpendicular equation of motion to be $\mathbf{p}_{j\perp} = -q_j \mathbf{A}$, and the parallel equation becomes

$$\frac{dp_{zj}}{dt} = -q_j \frac{\partial \phi}{\partial z} - m_j c^2 \frac{\partial \gamma_j}{\partial z}, \quad (\text{A.11})$$

where $\gamma_j = (1 + p_{zj}^2/m_j^2 c^2 + e^2 |\mathbf{A}|^2/m_j^2 c^2)^{1/2}$ is the relativistic ion gamma factor.

The dynamics of the electrons and ions in a collisionless plasma is given by the relativistic Vlasov equation for the electrons and ions. Assuming the plasma to be cold in the x - and y -directions, the particle distribution functions are $f_i(z, p_x, p_y, p_z, t) = f_i(z, v_z, t) \delta(p_x + eA_x) \delta(p_y + eA_y)$ and $f_e(z, p_x, p_y, p_z, t) = f_e(z, v_z, t) \delta(p_x - eA_x) \delta(p_y - eA_y)$, where δ is the Dirac delta function, and perform the integration in p_x and p_y space. As a result, the dynamics of the electrons and ions parallel to the laser beam is given by the relativistic electron and ion Vlasov equations, respectively,

$$\frac{\partial f_e}{\partial t} + \frac{p_z}{m_e \gamma_e} \frac{\partial f_e}{\partial z} + \frac{\partial(e\phi - m_e c^2 \gamma_e)}{\partial z} \frac{\partial f_e}{\partial p_z} = 0, \quad (\text{A.12})$$

and

$$\frac{\partial f_i}{\partial t} + \frac{p_z}{m_i \gamma_i} \frac{\partial f_i}{\partial z} + \frac{\partial(-e\phi - m_i c^2 \gamma_i)}{\partial z} \frac{\partial f_i}{\partial p_z} = 0. \quad (\text{A.13})$$

The Maxwell equation for the parallel electric field (A.8) and the electromagnetic wave equation (A.9) are, respectively,

$$\frac{\partial E_z}{\partial t} = \frac{e}{\epsilon_0} \int p_z \left(\frac{f_e}{m_e \gamma_e} - \frac{f_i}{m_i \gamma_i} \right) dp_z, \quad (\text{A.14})$$

and

$$\frac{\partial^2 \mathbf{A}}{\partial t^2} - \frac{\partial^2 \mathbf{A}}{\partial z^2} + \Omega_{pe}^2 \mathbf{A} = 0, \quad (\text{A.15})$$

where

$$\Omega_p^2 = \frac{e^2}{\epsilon_0} \int \left(\frac{f_e}{m_e \gamma_e} + \frac{f_i}{m_i \gamma_i} \right) dp_z \quad (\text{A.16})$$

represents the squared plasma frequency accounting for the electron and ion density variations and relativistic electron mass increase. The ion contribution is typically a factor m_i/m_e smaller than that of the electron contribution, and, in most cases, it can be safely neglected.

By using the Ansatz for the circularly polarized electromagnetic wave, viz. $\mathbf{A} = (1/2)A(z, t)(\hat{\mathbf{x}} + i\hat{\mathbf{y}}) \exp(-i\omega_0 t) + \text{complex conjugate}$, where ω_0 is the frequency, we have $|\mathbf{A}|^2 = |A|^2$ and we can write equation (A.15) as

$$\left(\frac{\partial}{\partial t} - i\omega_0 \right)^2 A - c^2 \frac{\partial^2 A}{\partial z^2} + \Omega_p^2 A = 0. \quad (\text{A.17})$$

In the limit of linearly polarized light, e.g. $\mathbf{A} = (1/2)A(z, t)\hat{\mathbf{x}} \exp(-i\omega_0 t) + \text{complex conjugate}$, equation (A.17) would still be valid, but we would have $|\mathbf{A}|^2 = |A|^2[1 + \cos(2\omega_0 t - 2\phi)]/2$, where ϕ is the complex phase of A . Hence, the ponderomotive force term will in this case have an oscillatory part with a frequency twice that of the laser light, which may lead to chaotic heating of the electrons [42, 43].

References

- [1] Shukla P K, Rao N N, Yu M Y and Tsintsadze N L 1986 Relativistic nonlinear effects in plasmas *Phys. Rep.* **138** 1–149
- [2] Bingham R, Mendonça J T and Shukla P K 2004 Plasma based charged-particle accelerators *Plasma Phys. Control. Fusion* **46** R1–23
- [3] Kodama R *et al* 2001 Fast heating of ultrahigh-density plasma as a step towards laser fusion ignition *Nature* **412** 798–802
- [4] Kodama R *et al* 2002 Nuclear fusion: fast heating scalable to laser fusion ignition *Nature* **418** 933–4
- [5] Tajima T and Dawson J M 1979 Laser electron accelerator *Phys. Rev. Lett.* **43** 267–70
- [6] Joshi C 2007 The development of laser- and beam-driven plasma accelerators as an experimental field *Phys. Plasmas* **14** 055501
- [7] Bingham R 2003 Accelerator physics: in the wake of success *Nature* **424** 258–9
- [8] Mangles S P D *et al* 2004 Monoenergetic beams of relativistic electrons from intense laserplasma interactions *Nature* **431** 535–8
- [9] Geddes C G R *et al* 2004 High-quality electron beams from a laser wakefield accelerator using plasma-channel guiding *Nature* **431** 538–41
- [10] Faure J *et al* 2004 A laserplasma accelerator producing monoenergetic electron beams *Nature* **431** 541–4
- [11] Tsung F S, Narang R, Mori W B, Joshi C, Fonseca R A and Silva L O 2004 Near-GeV-energy laser-wakefield acceleration of self-injected electrons in a centimeter-scale plasma channel *Phys. Rev. Lett.* **93** 185002
- [12] Hogan M J *et al* 2005 Multi-GeV energy gain in a plasma-wakefield accelerator *Phys. Rev. Lett.* **95** 054802
- [13] Leemans W P *et al* 2006 GeV electron beams from a centimetre-scale accelerator *Nat. Phys.* **2** 696–9
- [14] Lu W, Tzoufras M, Joshi C, Tsung F S, Mori W B, Vieira J, Fonseca R A and Silva L O 2007 Generating multi-GeV electron bunches using single stage laser wakefield acceleration in a 3D nonlinear regime *Phys. Rev. ST Accel. Beams* **10** 061301
- [15] Blumenfeld I *et al* 2007 Energy doubling of 42 GeV electrons in a metre-scale plasma wakefield accelerator *Nature* **445** 741–4
- [16] Bingham R 2007 Plasma physics: on the crest of a wake *Nature* **445** 721–2
- [17] Jones B 2005 The case for particle therapy *Br. J. Radiol.* **79** 24–31
- [18] Jones B and Burnet N 2005 Radiotherapy for the future *Br. Med. J.* **330** 979–80
- [19] Ledingham K W D, Galster W and Sauerbrey R 2007 Laser-driven proton oncology—a unique new cancer therapy? *Br. J. Radiol.* **80** 855–8
- [20] Fourkal E, Veltchev I and Ma C-M 2009 Laser-to-proton energy transfer efficiency in laser-plasma interactions *J. Plasma Phys.* **75** 235–50
- [21] Schwoefer H, Pfoth S, Jäckel O, Amthor K-U, Liesfeld B, Ziegler W, Sauerbrey R, Ledingham K W D and Esirkepov T 2006 Laser-plasma acceleration of quasi-monoenergetic protons from microstructured targets *Nature* **439** 445–8
- [22] Hegelich B M, Albright B J, Cobble J, Flippo K, Letzring S, Paffett M, Ruhl H, Schreiber J, Schulze R K and Fernandez J C 2006 Laser acceleration of quasi-monoenergetic MeV ion beams *Nature* **439** 441–4
- [23] Fuchs J *et al* 2007 Laser-foil acceleration of high-energy protons in small-scale plasma gradients *Phys. Rev. Lett.* **99** 015002
- [24] Hatchett S P *et al* 2000 Electron, photon, and ion beams from the relativistic interaction of Petawatt laser pulses with solid targets *Phys. Plasmas* **7** 2076

- [25] Wilks S C, Langdon A B, Cowan T E, Roth M, Singh M, Hatchett S, Key M H, Pennington D, MacKinnon A and Snavely R A 2001 Energetic proton generation in ultra-intense laser-solid interactions *Phys. Plasmas* **8** 542–9
- [26] Krushelnick K *et al* 1999 Multi-MeV ion production from high-intensity laser interactions with underdense plasmas *Phys. Rev. Lett.* **83** 737–40
- [27] Sentoku Y *et al* 2000 High density collimated beams of relativistic ions produced by petawatt laser pulses in plasmas *Phys. Rev. E* **62** 7271–81
- [28] Bulanov S V *et al* 2002 Generation of high-quality charged particle beams during the acceleration of ions by high-power laser radiation *Plasma Phys. Rep.* **28** 975–91
- [29] Silva L O *et al* 2004 Proton shock acceleration in laser–plasma interactions *Phys. Rev. Lett.* **92** 015002
- [30] Zhou C T and He X T 2007 Influence of a large oblique incident angle on energetic protons accelerated from solid-density plasmas by ultraintense laser pulses *Appl. Phys. Lett.* **96** 031503
- [31] Mora P 2007 Laser driven ion acceleration *AIP Conf. Proc.* **920** 98–117
- [32] Lee K *et al* 2008 Generation of intense proton beams from plastic targets irradiated by an ultraintense laser pulse *Phys. Rev. E* **78** 056403
- [33] Robson L *et al* 2007 Scaling of proton acceleration driven by petawatt–laser–plasma interactions *Nat. Phys.* **3** 58–62
- [34] Antici P, Fuchs J, d’Humières E, Robiche J, Brambrink E, Atzeni S, Schiavi A, Sentoku Y, Audebert P and Pépin P 2009 Laser acceleration of high-energy protons in variable density plasmas *New J. Phys.* **11** 023038
- [35] Dong Q L, Sheng Z-M, Yu M Y and Zhang J 2003 Optimization of ion acceleration in the interaction of intense femtosecond laser pulses with ultrathin foils *Phys. Rev. E* **68** 026408
- [36] Passoni M and Lontano M 2008 Theory of light-ion acceleration driven by a strong charge separation *Phys. Rev. Lett.* **101** 115001
- [37] Esirkepov T, Borghesi M, Bulanov S V, Mourou G and Tajima T 2004 Highly efficient relativistic-ion generation in the laser-piston regime *Phys. Rev. Lett.* **92** 175003
- [38] d’Humières E, Lefebvre E and Gremillet L 2005 Proton acceleration mechanisms in high-density laser interaction with thin foils *Phys. Plasmas* **12** 062704
- [39] Yin L, Albright B J, Hegelich B M, Bowers K J, Flippo K A, Kwan T J T and Fernández J C 2007 Monoenergetic and GeV ion acceleration from the laser breakout afterburner using ultrathin foil *Phys. Plasmas* **14** 056706
- [40] Macchi A, Cattani F, Liseykina T V and Cornolti F 2005 Laser acceleration of ion bunches at the front surface of overdense plasmas *Phys. Rev. Lett.* **94** 165003
- [41] Klimo O, Psikal J, Limpouch J and Tikhonchuk V T 2008 Monoenergetic ion beams from ultrathin foils irradiated by ultrahigh-contrast circularly polarized laser pulses *Phys. Rev. ST Accel. Beams* **11** 031301
- [42] Robinson A P L, Zepf M, Kar S, Evans R G and Bellei C 2009 Radiation pressure acceleration of thin foils with circularly polarized laser pulses *New J. Phys.* **10** 013021
- [43] Rykovanov S G, Schreiber J, Meyer-ter-Vehn J, Bellei C, Henig A, Wu H C and Geissler M 2008 Ion acceleration with ultra-thin foils using elliptically polarized laser beams *New J. Phys.* **10** 113005
- [44] Yan X Q, Lin C and Sheng Z M 2008 Generating High-current monoenergetic proton beams by a circularly polarized laser pulse in the phase-stable acceleration regime *Phys. Rev. Lett.* **100** 135003
- [45] Liseykina T V, Borghesi M, Macchi A and Tuveri S 2008 Radiation pressure acceleration by ultraintense laser pulses *Plasma Phys. Control. Fusion* **50** 124033
- [46] Pegoraro F and Bulanov S V 2007 Photon bubbles and ion acceleration in a plasma dominated the radiation pressure of an electromagnetic pulse *Phys. Rev. Lett.* **99** 065002
- [47] Tripathi V K, Liu C S, Shao X, Eliasson B and Sagdeev R Z 2009 Laser acceleration of monoenergetic protons in a self-organized double layer from thin foil *Plasma Phys. Control. Fusion* **51** 024014
- [48] Einstein A 1905 Zur elektrodynamik bewegter Körper *Ann. Phys., Lpz.* **17** 891–921
- [49] Censor D 1971 Energy balance and radiation forces for arbitrary moving objects *Radio Sci.* **6** 903

- [50] Landau L D and Lifshitz E M 1980 *The Classical Theory of Fields* (Oxford: Pergamon)
- [51] Pauli W 1981 *Theory of Relativity* (New York: Dover)
- [52] Debye P 1909 Der lichtdruck auf kugeln von beliebigen material *Ann. Phys., Lpz.* **30** 57–136
- [53] Marx G 1966 Interstellar vehicle propelled by terrestrial laser beam *Nature* **211** 22–3
- [54] Birdsall C K and Langdon A B 1991 *Plasma Physics Via Computer Simulation* (Bristol: Institute of Physics)
- [55] Arber T and Vann R G L 2002 A critical comparison of Eulerian-grid-based Vlasov solvers *J. Comput. Phys.* **180** 339–57
- [56] Bertrand P, Ghizzo A, Karttunen S J, Pättikangas T J H, Salomaa R R E and Shoucri M 1995 Two-stage electron acceleration by simultaneous stimulated Raman backward and forward scattering *Phys. Plasmas* **2** 3115
- [57] Huot F, Ghizzo A, Bertrand P, Sonnendrücker E and Coulaud O 2003 Instability of the time splitting scheme for the one-dimensional and relativistic Vlasov–Maxwell system *J. Comput. Phys.* **185** 512–31
- [58] Shukla P K and Eliasson B 2005 Localization of intense electromagnetic waves in a relativistically hot plasma *Phys. Rev. Lett.* **94** 065002
- [59] Eliasson B, Liu C S, Shukla P K and Kumar N 2006 Dynamics of relativistic laser pulses in plasmas *Phys. Scr.* **73** 632–8
- [60] Lele S K 1992 Compact finite difference schemes with spectral-like resolution *J. Comput. Phys.* **103** 16–42